3*d* oxide molecules to tailor large magnetic anisotropy energies on MgO films

Sufyan Shehada [1,2,3,*] Manuel dos Santos Dias [1,4,5] Muayad Abusaa [3] and Samir Lounis [1,4,†]

[1]*Peter Grünberg Institut, Forschungszentrum Jülich and JARA, D-52425 Jülich, Germany*

[2]*RWTH Aachen University, 52056 Aachen, Germany*

[3]*Department of Physics, Arab American University, 240 Jenin, Palestine*

[4]*Faculty of Physics, University of Duisburg-Essen and CENIDE, 47053 Duisburg, Germany*

[5]*Scientific Computing Department, STFC Daresbury Laboratory, Warrington WA4 4AD, United Kingdom*

(Received 27 March 2024; revised 8 November 2024; accepted 25 November 2024; published 4 December 2024)

Designing systems with large magnetic anisotropy energy (MAE) is desirable and critical for nanoscale magnetic devices. A recent breakthrough achieved the theoretical limit of the MAE for 3*d* transition metal atoms by placing a single Co atom on a MgO(100) surface, a result not replicated by standard first-principles simulations. Our paper, incorporating Hubbard-*U* correction and spin-orbit coupling, successfully reproduces and explains the high MAE of a Co adatom on a MgO (001) surface. We go further by exploring ways to enhance MAE in 3*d* transition metal adatoms through different structural geometries of 3*d*−O molecules on MgO. One promising structure, with molecules perpendicular to the surface, enhances MAE while reducing substrate interaction, minimizing spin fluctuations, and boosting magnetic stability. Additionally, we demonstrate significant control over MAE by precisely placing 3*d*−O molecules on the substrate at the atomic level.

DOI: 10.1103/PhysRevB.110.224409

I. INTRODUCTION

Surface-embedded molecular magnetic structures are of tremendous interest, as they represent the smallest magnetic units at the ultimate atomic scale [1–3]. Recent studies on magnetic adatoms with sizable magnetic anisotropy energy (MAE) has been intense due to their potential applications in high-density information storage and quantum spin processing [4–13]. For nanostructures on surfaces, the MAE is typically dominated by its uniaxial contribution, which can be computed from the energy difference between having the spin moment perpendicular to and in the surface plane: $K = E(\mathbf{S} \parallel \hat{\mathbf{z}}) - E(\mathbf{S} \parallel \hat{\mathbf{x}})$. For instance, single Co atoms deposited onto a Pt (111) surface give rise to an out-of-plane MAE of about −9 meV per adatom favoring an out-of-plane orientation of the magnetic moment, and the assembled Co nanoparticles have an MAE that is reliant on the coordination of a single atom [4] while being enhanced by the polarization of the substrate [14]. If the Co atoms are separated from the Pt surface by graphene, the MAE is maintained at a significant value (MAE =+8.1 meV per adatom, where the positive sign indicates an in-plane MAE) [7]. *Ab initio* simulations predicted the possibility of achieving remarkable MAEs for Co or Ir dimers on graphene (MAE = −30 meV per adatom) [8], for Os adatoms on graphene nanoflakes (MAE = −22 meV per adatom) [9], and for Co dimers on benzene (MAE = −50 meV per adatom) [10]. A substantial out-of-plane MAE would generate an energy barrier that could protect the magnetization from thermal or quantum fluctuations [15–17], making it robust and stable and allowing the magnetization to be orientated in a preferred spatial direction for a sufficient duration of time, which would be practical for the realization of a magnetic bit. It is also interesting to note that the values of the MAE obtained for these few-atom systems can be much higher than the ones found in well-known magnets such as hcp Co ($K \sim -0.06$ meV per atom) and $L1_0$ FePt ($K \sim -2$ meV per Fe atom) [18], which points to underlying microscopic differences in how the MAE is established and that we explore in this paper.

Strategies for enhancing the MAE of magnetic adatoms are based on three vital aspects: a large spin-orbit coupling (SOC) energy, a significant orbital moment, and a special ligand field [11,12,15,19,20]. As a ligand field frequently quenches or reduces an orbital moment, by enforcing orbital degeneracies, it is difficult to attain a massive MAE without a suitable surface or substrate. Recently, thin insulating layers of MgO developed into an appealing substrate for exploring various magnetic aspects pertaining to magnetic adatoms and molecules [11,13,19,21–43].

On that very substrate, Rau *et al.* [11] discovered that a Co adatom adsorbing on the oxygen-top position of the MgO (001) surface (see Fig. 1) is characterized by a large MAE since the underlying measured zero-field splitting with inelastic scanning tunneling spectroscopy reaches approximately 60 meV [11]. Assuming a spin $\frac{3}{2}$ for the Co adatom implied a MAE of the order of −90 meV per adatom [44], which broke records and reached the magnetic anisotropy limit of

*Contact author: s.shehada@fz-juelich.de

†Contact author: s.lounis@fz-juelich.de

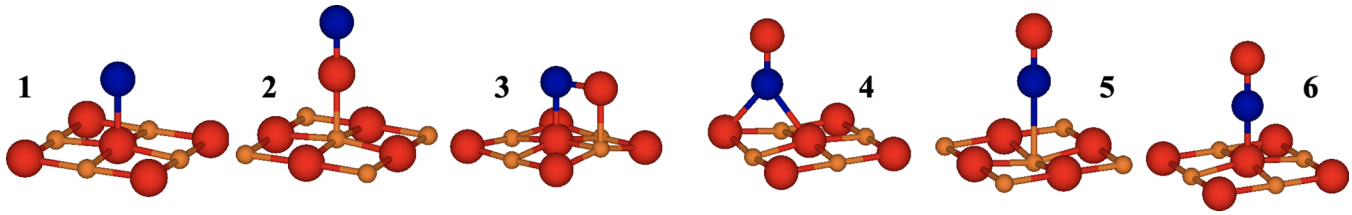

FIG. 1. Investigated atomic structures for 3*d* adatom and 3*d*−O molecules on a bilayer of MgO. The different structures are numbered depending on the orientation of the molecule with respect to the substrate. 3*d* atoms are represented by blue spheres, O by red spheres, and Mg by orange spheres.

3*d* transition metals. Details of the interaction between the Co and MgO surface, for instance, the Co–O bond, uniquely determines the underlying magnetic properties. In our current paper, we observe that conventional density functional theory (DFT) simulations using the local spin-density approximation (LSDA) or generalized gradient approximation (GGA) do not recover the large MAE of Co on MgO. Ou *et al.* [44] predicted that orbital reordering as described within DFT + U can occur, which can enhance the MAE of Co on MgO while leading to gigantic MAEs for Ru (MAE = −110 meV per adatom) and Os on the same surface (MAE = −208 meV per adatom).

In this paper, we investigate from *ab initio* (see Methods section) the remarkable MAE of Co, in particular, and the underlying electronic mechanisms leading to its large value. Furthermore, we explore the MAE of the whole series of 3*d* adatoms on the MgO surface with the aim of identifying the ideal structural scenario for enhancing their MAE by forming molecules with an additional O atom (XO molecules, X being a 3*d* atom); see Fig. 1. Of our particular interest is the case where the molecule is perpendicular to the MgO surface, such that the interaction of Co with the substrate is minimized, as shown in Figs. 1 and 2, which should reduce the substrate-induced spin fluctuations to a minimum [15].

II. MAE OF A SINGLE CO ADATOM ON THE BILAYER OF MgO

To set the stage for our study, we investigate the MAE of a single Co adatom on a bilayer of MgO surface. We consider the adatom on an O-top site (see Fig. 1) since it is the most stable adsorption site [11,31]. Regular LSDA calculations lead to a weak MAE (−10 meV per adatom), which favors an out-of-plane orientation of the magnetic moment. Since electronic correlations are expected to be crucial on MgO, we incorporated different values of the Hubbard U (and exchange parameter J) including SOC. Once correlations are taken into account, the MAE experiences a large increase and reaches the order of magnitude experimental values for $U = 4$ eV, $J = 1$ eV (MAE = −145.2 meV per adatom), and for $U = 6$ eV, $J = 1$ eV (MAE = −93.3 meV per adatom).

To understand the underlying physics, we plot the corresponding partial density of states (PDOS) of a Co adatom without including SOC (Fig. 2). A common feature in all investigated cases is the degeneracy at the Fermi level of the d_{xz} and d_{yz} states. The rest of the states experience clear shifts with respect to the Fermi energy as soon as the Hubbard-U correction is included, which presumably triggers the aforementioned differences in the MAE. In the following, we utilize degenerate first-order and nondegenerate second-order perturbation theories [45–48] to unveil the mechanisms shaping the large MAE characterizing the Co adatom.

A. First-order degenerate perturbation theory

In our discussion, first we focus on the case of $U = 0$ eV and $J = 0$ eV. We start by looking at the PDOS for the d states in Fig. 2(a). As aforementioned, the d_{xz} and d_{yz} minority-spin states are degenerate at the Fermi level for which we have to proceed with first-order degenerate perturbation theory [48–51] to predict the impact of spin-orbit coupling. The z component of the orbital momentum operator is the only one connecting both orbitals, implying that the SOC term of interest is $\frac{1}{2}\xi\sigma_z \cdot \hat{\mathbf{L}}_z$, which simplifies to $-\frac{1}{2}\xi\hat{L}_z$ since the two states are of minority-spin character. Here ξ is the radial integral of the SOC with the associated atomic wave functions. This also means that there is gain in energy only when the moment points along the z direction. We diagonalize the degenerate subspace including the SOC term,

$$\begin{bmatrix} \hat{H}_{11} & \hat{H}_{12} \\ \hat{H}_{21} & \hat{H}_{22} \end{bmatrix} = -\frac{1}{2}\xi \begin{bmatrix} 0 & \langle d_{xz}|\,\hat{L}_z\,|d_{yz}\rangle \\ \langle d_{yz}|\,\hat{L}_z\,|d_{xz}\rangle & 0 \end{bmatrix} = -\frac{1}{2}\xi \begin{bmatrix} 0 & -\mathrm{i} \\ \mathrm{i} & 0 \end{bmatrix}, \quad (1)$$

and find as eigenvalues

$$\Delta \mathrm{E}_{\pm} = \mp\tfrac{1}{2}\xi\,. \quad (2)$$

The corresponding eigenstates are $[d_1^{\downarrow} = \frac{1}{\sqrt{2}}(d_{xz} + i\,d_{yz})]$ for eigenvalue $\mathrm{E}_1 = -\frac{1}{2}\xi$, which carries an orbital moment of 1 μ_B and $[d_2^{\downarrow} = \frac{1}{\sqrt{2}}(d_{xz} - i\,d_{yz})]$ for eigenvalue $\mathrm{E}_2 = \frac{1}{2}\xi$ with an orbital moment of −1 μ_B. The electron initially shared by both orbitals d_{xz} and d_{yz} located at the Fermi energy will be located in the lowest energy state associated to $d_1^{\downarrow}$ just below the Fermi energy while the $d_2^{\downarrow}$ state becomes unoccupied.

Overall, we conclude that the easy axis along z direction is strongly favored by the degenerate states located at the Fermi energy, contributing to the MAE by a large value of $\mathrm{MAE}_{1^{\mathrm{st}}\mathrm{order}} = -\frac{1}{2}\xi = -35$ meV, where we assumed that $\xi \approx 70$ meV for Co [52]. Obviously, it is the degeneracy of the d_{xz} and d_{yz} minority-spin states at the Fermi energy, which is responsible for the large out-of-plane MAE detected experimentally. The differences noticed among the simulations

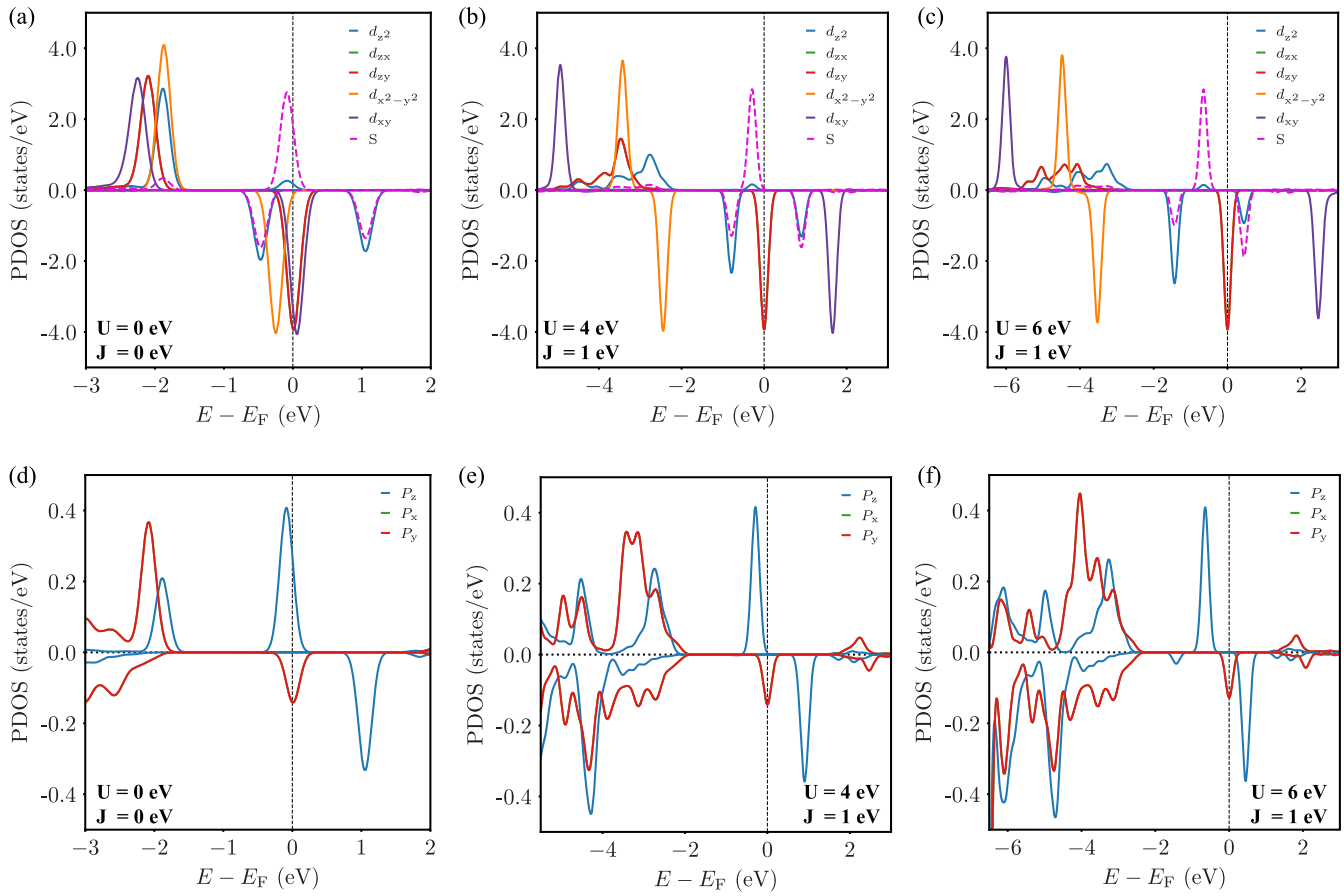

FIG. 2. Effect of the Hubbard-U correction on the electronic structure of a Co adatom (a)–(c) atop oxygen (d)–(f) from the MgO bilayer of MgO in the absence of SOC. (a), (d) PDOS for $U = 0$ eV and $J = 0$ eV; (b), (e) PDOS for $U = 4$ eV and $J = 1$ eV; (c), (f) PDOS for $U = 6$ eV and $J = 1$ eV. The Fermi energy is marked by a vertical dashed line. The lower part of each panel shows (the negative of) PDOS for spin down and the upper part PDOS for spin- up. The zx PDOS is not visible in the plots in Fig. 2 because the zx and yz states are degenerate.

utilizing various values of U and J must be induced by the rest of the states, which are nondegenerate. These will be addressed in the following.

B. Second-order nondegenerate perturbation theory

Here we evaluate the contributions to the MAE from the nondegenerate states. The MAE is determined by the matrix elements of SOC involving occupied and unoccupied states [45],

$$\mathrm{MAE}_{2^{\mathrm{nd}}\mathrm{order}} = \frac{\xi^2}{4} \sum_{o,u,\sigma,\sigma'} (1 - 2\delta_{\sigma\sigma'}) \times \frac{|\langle o^\sigma|\hat{L}_z|u^{\sigma'}\rangle|^2 - |\langle o^\sigma|\hat{L}_x|u^{\sigma'}\rangle|^2}{\epsilon_{u,\sigma'} - \epsilon_{o,\sigma}}, \tag{3}$$

where $o^\sigma\,(u^{\sigma'})$ and $\epsilon_{o,\sigma}\,(\epsilon_{u,\sigma'})$ represent eigenstates and eigenvalues of occupied (unoccupied) states in spin state $\sigma(\sigma')$. The nonzero $\hat{L}_z$ and $\hat{L}_x$ matrix elements involving d states are $|\langle d_{xz}|\hat{L}_z|d_{yz}\rangle|^2 = 1$, $|\langle d_{x^2-y^2}|\hat{L}_z|d_{xy}\rangle|^2 = 4$, $|\langle d_{z^2}|\hat{L}_x|d_{xz}, d_{yz}\rangle|^2 = 3$, $|\langle d_{xy}|\hat{L}_x|d_{xz}, d_{yz}\rangle|^2 = 1$, and $|\langle d_{x^2-y^2}|\hat{L}_x|d_{xz}, d_{yz}\rangle|^2 = 1$. Considering that all the majority-spin states are fully occupied and rather far away from the Fermi energy, as shown in Fig. 2, the dominant contribution to the MAE can be attributed to the minority-spin states, spin-down occupied and spin-down unoccupied states, $\sigma(\sigma') = (\downarrow\downarrow)$. We neglect spin-flip contributions from spin-up occupied and spin-down unoccupied states for the qualitative analysis carried out in this section. The discrete energies used in the MAE calculation are identified as the positions of the PDOS peaks of the Co atom in Fig. 2. In fact, there is a satellite majority-spin d_{z^2} state showing up close to the Fermi energy. However, it emerges from the p_z state of the underlying oxygen atom, which gives rise to a prominent s state (shown as a dashed line in Fig. 2). Equation (3) is characterized by three primary finite dominant factors,

$$\mathrm{MAE}_{2^{\mathrm{nd}}\mathrm{order}} = -\frac{\xi^2}{4}\frac{|\langle d^\downarrow_{x^2-y^2}|\hat{L}_z|d^\downarrow_{xy}\rangle|^2}{\epsilon_{xy,\downarrow} - \epsilon_{x^2-y^2,\downarrow}} + \frac{\xi^2}{4}\frac{|\langle d^\downarrow_1|\hat{L}_x|d^\downarrow_{z^2}\rangle|^2}{\epsilon_{z^2,\downarrow} - \epsilon_{1,\downarrow}} + \frac{\xi^2}{4}\frac{|\langle d^\downarrow_1|\hat{L}_x|d^\downarrow_{xy}\rangle|^2}{\epsilon_{xy,\downarrow} - \epsilon_{1,\downarrow}}, \tag{4}$$

which are listed in Table I for different values of U and J and compared to the value obtained from first-order degenerate perturbation theory. Since static correlations increase the energy splitting between the occupied $d^\downarrow_{x^2-y^2}$ and unoccupied

TABLE I. Various contributions from first-order degenerate and second-order nondegenerate perturbation theories to the MAE of Co adatom on the bilayer of MgO in the oxygen-top position from DFT+U with the absence of SOC. A negative sign of the MAE favors an out-of-plane magnetization. U and J are given in eV, while the MAE is in meV.

MAE	$U=0$, $J=0$	$U=4$, $J=1$	$U=6$, $J=1$
$-\frac{\xi^2}{4}\frac{\lvert\langle d^{\downarrow}_{x^2-y^2}\rvert\hat{L_z}\rvert d^{\downarrow}_{xy}\rangle\rvert^2}{\epsilon_{xy,\downarrow}-\epsilon_{x^2-y^2,\downarrow}}$	−15.75	−1.19	−0.82
$+\frac{\xi^2}{4}\frac{\lvert\langle d^{\downarrow}_{1}\rvert\hat{L_x}\rvert d^{\downarrow}_{z^2}\rangle\rvert^2}{\epsilon_{z^2,\downarrow}-\epsilon_{1,\downarrow}}$	6.97	8.13	16.73
$+\frac{\xi^2}{4}\frac{\lvert\langle d^{\downarrow}_{1}\rvert\hat{L_x}\rvert d^{\downarrow}_{xy}\rangle\rvert^2}{\epsilon_{xy,\downarrow}-\epsilon_{1,\downarrow}}$	38.89	1.47	1.00
$\mathrm{MAE}_{1^{\mathrm{st}}\mathrm{order}}=-\frac{1}{2}\xi$	−35.0	−35.0	−35.0
$\mathrm{MAE}_{1^{\mathrm{st}}\mathrm{order}}+\mathrm{MAE}_{2^{\mathrm{nd}}\mathrm{order}}$	−4.90	−26.59	−18.08

$d^{\downarrow}_{xy}$, the first term in Eq. (3), favoring the out-of-plane easy axis, reduces in magnitude. The same trend is followed by the third term, which, however, favors an in-plane orientation of the moment in contrast to the second term. Clearly, there is complex competition between the different terms, which imposes a reduction of the MAE emerging from first-order degenerate perturbation theory. After summing up the different contributions to the MAE as obtained from first- and second-order perturbation theory, we recover qualitatively the trends found from the full *ab initio* calculations as reported in Table I. This shows that the main mechanism favoring the out-of-plane orientation of the magnetic moment with a large MAE is driven by the SOC-induced lifting of the degeneracy of the minority-spin d_{xz} and d_{yz} states located at the Fermi energy. We note that the magnitude of the predicted MAE is of the same order than the one obtained by a previous theoretical study [44] based on full-potential augmented plane wave calculations. Their argument, however, to explain the large MAE of the Co adatom is different from ours and is based on a nontrivial reordering of the occupation matrix generated with static correlations.

In the next section, we investigate the MAE of the rest of the 3d series of adatoms deposited on MgO and explore the possibility of enhancing their MAE by considering 3d−O molecules as potential adsorbates (see Fig. 1). In the following, we limit our simulations incorporating correlations to the case of $U=6$ eV and $J=1$ eV since the MAE value obtained

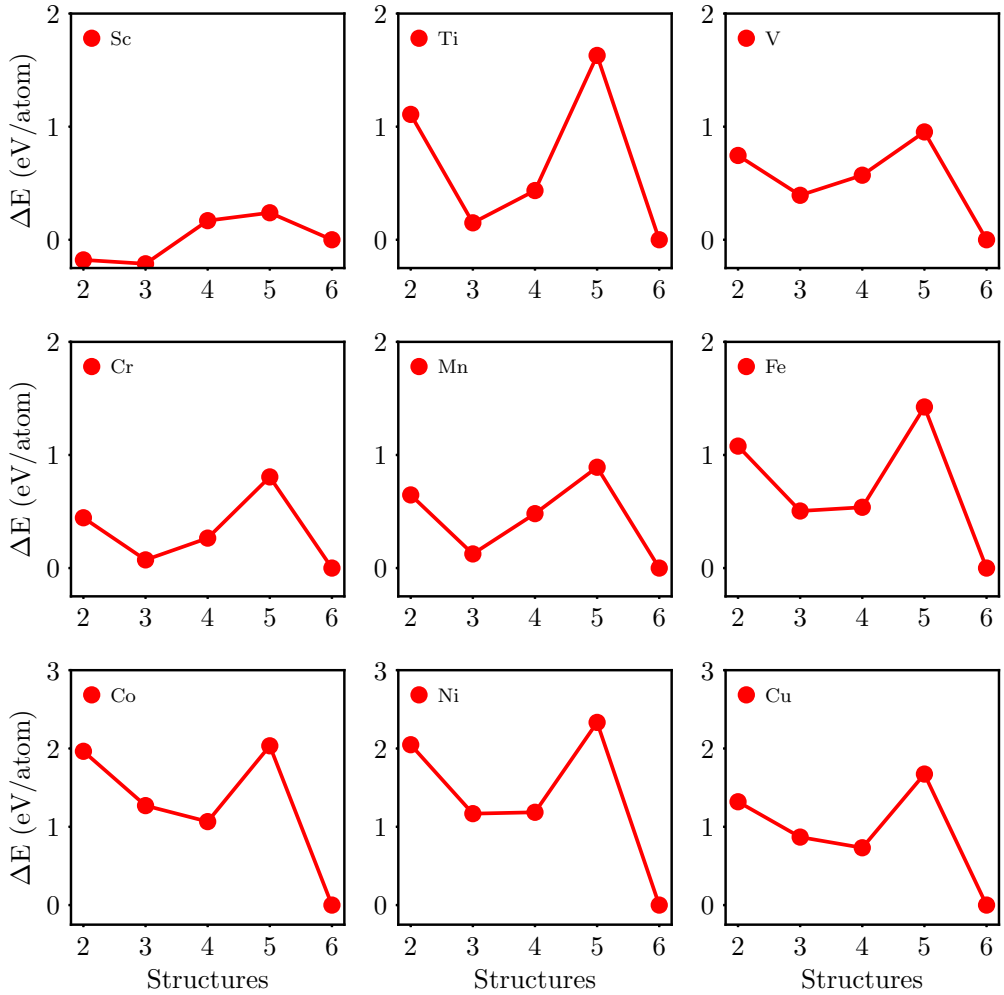

FIG. 3. Total energy difference of 3d−O molecules on the bilayer of MgO with respect to the one of structure 6. The structure number indicates a particular nanostructure illustrated in Fig. 1.

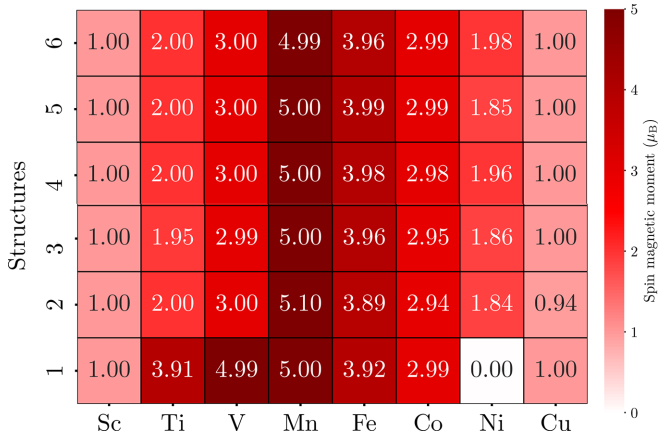

FIG. 4. Spin magnetic moments of 3d adatoms and 3d−O molecules on a bilayer of MgO. The structure number indicates a particular nanostructure with a specific orientation of the magnetization as illustrated in Fig. 1.

for a Co adatom is the closest to the experimentally measured one [11].

III. MAE of 3d ADATOMS AND 3d−O MOLECULES ON THE BILAYER OF MgO

Here, we address the main topic of our investigation, namely, 3d adatoms on the bilayer of MgO and the 3d−O molecules placed on the MgO bilayer considering different structures. After structural relaxation, using LSDA+U ($U = 6$ eV and $J = 1$ eV) total energy calculations, we classified the results into six structures shown in Fig. 1. As illustrated in Fig. 3, structure 6 is energetically the most favorable one for all 3d−O molecules except for the Sc–O molecule case, while structure 5 is the one that is the least favorable. Independent from their relative stability, we study the MAE of all the converged nanostructures.

Most of the investigated structures have C_{4V} symmetry except for structures 3 and 4. For the latter cases, we explore two in-plane rotations of the magnetization and calculate the MAE by taking the energy difference $\mathrm{MAE} = \mathrm{E}^{\hat{z}} - \mathrm{E}^{\phi}$, where ϕ is the azimuthal angle. The cases where the magnetic moment points in-plane with an azimuthal angle $\phi = 0°$, $\phi = 45°$, and $\phi = 90°$ are, respectively, denoted a, b, and c. These angles correspond to the [100], [110], and [010] directions of the MgO surface.

It is valuable to explore how the magnetic moments of the 3d atoms are changed once embedded in the 3d−O molecules as summarized in Fig. 4. Among all investigated nanostructures, only three single adatoms do not follow Hund's first rule: Ni, Ti, and V. The spin moments of the different deposited nanostructures are generally unaffected by the positions of the 3d−O molecules and the electronic occupation is consistent with a nominal valence of $[\mathrm{Ar}]4s^2 3d^n$. We note that Cr is not considered in the current paper for MAE analysis. While we successfully obtained the structural properties for Cr and CrO on MgO, we encountered convergence issues during the MAE calculations due to the inclusion of SOC. This prevented us from achieving reliable MAE values for Cr. Its MAE is expected to be nevertheless negligible.

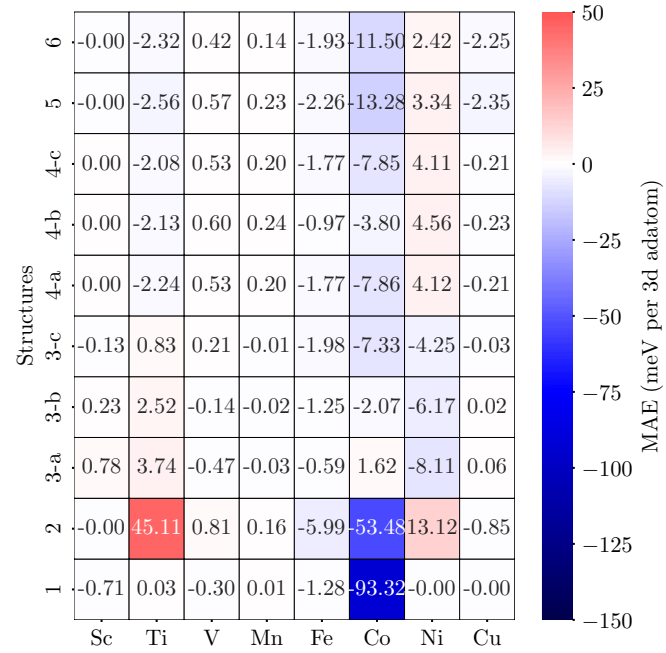

FIG. 5. MAE of 3d adatoms and 3d−O molecules on a bilayer of MgO, expressed in meV per 3d adatom. The structure number indicates a particular nanostructure with a specific orientation of the magnetization as illustrated in Fig. 1. Configurations a, b, and c correspond to the energy differences evaluated when the moment is rotated in plane with the azimuthal angles $\phi = 0°$, $\phi = 45°$, and $\phi = 90°$, respectively. Positive MAE values indicate a preference for in-plane magnetization, while negative values favor out-of-plane magnetization.

The calculated MAEs are presented in Fig. 5. Ti, Fe, Co, and Ni structures generally yield significant MAE ranging from a few to tens meV per adatom. At the same time, the MAE values of Sc, V, Mn, and Cu are close to zero for all structures except the Cu–O molecule, which is characterized by an out-of-plane MAE of 2.35 and 2.25 meV per adatom in structures 5 and 6, respectively.

Among all the 3d adatoms and 3d−O molecules, a single Co adatom on the bilayer of MgO in the oxygen-top position exhibits the most significant MAE values (an out-of-plane MAE of −93 meV per adatom), representing the magnetic anisotropy limit of 3d adatoms and 3d−O molecules on MgO as obtained from our simulations. Moreover, Co–O molecule in structure 2 (see Figs. 1 and 2) is perpendicular to the substrate and has the second largest out-of-plane MAE of 53 meV per adatom compared to the rest of the explored nanostructures; see Fig. 5. A closer look at the Ti MAE values in Fig. 5 reveals that the perpendicular Ti–O molecule in structure 2 has the largest in-plane MAE of 45 meV per adatom, with the remaining structures' MAE values significantly decreasing (range between 0 and 4 meV per adatom). Except for structure 3-a, Co–O molecules prefer an out-of-plane orientation of the magnetization.

We expect structure 2, to be the one where the 3d atoms are less interacting with the substrate, which should favor magnetic stability if allowed by the right out-of-plane MAE. In principle, its MAE should be close to the freestanding

TABLE II. MAE of the isolated Co–O molecule for different bond lengths between Co and O atoms (d_{Co-O}). CoO/2MgO is the perpendicular Co–O molecule on the MgO bilayer (see Figs. 1 and 2). The MAE values are given in meV per adatom. A negative sign of the MAE favors an out-of-plane magnetization. Here we used $U = 6$ eV and $J = 1$ eV.

d_{Co-O}(Å)	1.7	1.8	1.9	2	CoO/2MgO
MAE (meV)	−46.06	−48.25	−50.89	−52.11	−53.48

molecule. To examine this scenario, we calculated the MAE of the isolated Co–O molecule for different bond lengths between Co and O atoms (d_{Co-O}), see Table II, to cover all the bond lengths of Co–O molecules on the bilayer of MgO (structures 2–6 in Fig. 1). Table II shows excellent agreement between the computed MAE of the isolated Co–O molecule and the perpendicular Co–O molecule on the MgO bilayer, which confirms our expectations. Moreover, Table II reveals a minimal effect of the bond length on the computed MAEs of the isolated Co–O molecule.

The perpendicular Co–O molecule (structure 2 in Fig. 1) with a large MAE is energetically less stable than the horizontal one (structure 3 in Fig. 1) with a weaker MAE. However, our simulations indicate that the perpendicular molecule is metastable and could be protected by an energy barrier, preventing it from falling into the horizontal configuration and would enable its experimental realization. Figure 6 shows the energy difference associated to the rotation of the molecule on MgO, where a large barrier of 0.6 eV can be clearly recognized.

IV. CONCLUSION

We presented the results of *ab initio* calculations on the MAE of $3d-$O molecules freestanding or deposited on the MgO bilayer, which were compared to the case of $3d$ adatoms on the oxygen-top position of the MgO bilayer. We explored, in particular, their structural, electronic, and magnetic properties, and scrutinized the impact of the existence of an extra oxygen atom attached to $3d$ adatoms on the MAE. The physics of the latter is mainly explained by applying degenerate and nondegenerate perturbation theories.

We evidenced the ability to substantially modify the MAE via atomic control of the location of the $3d-$O molecules on the bilayer of MgO substrate. In particular, we revealed the possibility of having the $3d-$O molecules perpendicular to the substrate with the $3d$ adatom being atop the oxygen atom of the molecule, which should minimize spin fluctuations triggered by the interaction with the substrate. These molecules can be characterized by large MAE similar to that of the isolated Co adatom. Both aspects, large MAE and weak coupling to the substrate are the right ingredients to enable magnetic stability of the nanostructure, which so far has not been achieved for $3d$ adatoms, to the best of our knowledge. In fact, the perpendicular $3d-$O molecules on the bilayer of MgO act like the isolated $3d-$O molecule indicating the weak impact of the substrate on the MAE, especially in the cases of Co–O, Ti–O, Ni–O, and Fe–O perpendicular molecules. Although the aforementioned perpendicular molecule is a metastable structure, it could be protected by an energy barrier, which makes its experimental realization via atomic manipulation with scanning tunneling microscopy possible. Moreover, we evidenced the ability to substantially modify the MAE by atomic control by controlling the location of the $3d-$O molecules on the substrate.

V. METHODS

The simulations are conducted within density functional theory as implemented in the QUANTUM ESPRESSO code with scalar relativistic [53] as well as fully relativistic ultrasoft pseudopotentials (USPPs) [54,55]. We assume the LSDA [56] and consider electronic correlations within the formulation of the Hubbard-U correction based on Refs. [57–59].

We apply two formulations of the Hubbard-U correction in this paper: (i) Dudarev's approach [58,59] used for structure relaxation and (ii) Liechtenstein's formulation [57] used for MAE calculations. We utilize this hybrid scheme because of their current implementations and stability in the QUANTUM ESPRESSO code. First, Dudarev's approach is suitable for SOC and atomic relaxations but currently incompatible with

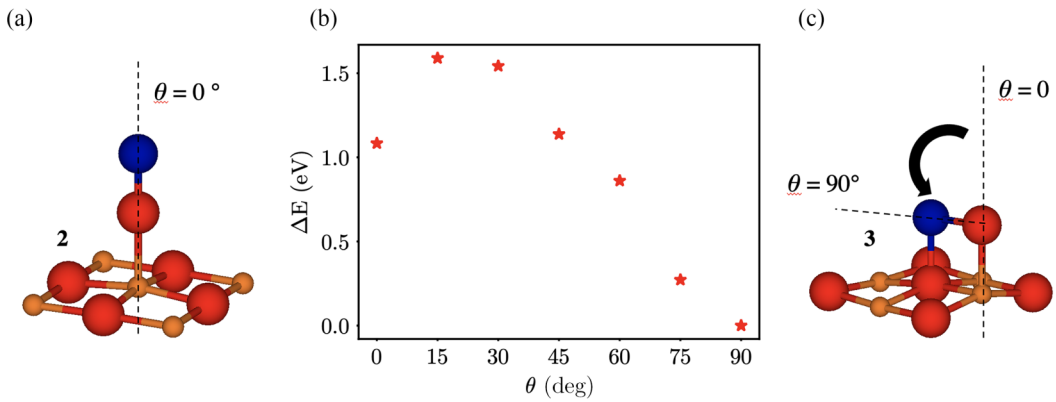

FIG. 6. Energy barrier for the metastable perpendicular Co–O molecule on the bilayer of MgO. (a) The perpendicular Co–O molecule on the MgO bilayer ($\theta = 0°$); (b) total energy difference of Co–O molecule on the bilayer of MgO with respect to structure 3, as a function of the rotation angle (θ); and (c) the horizontal Co–O molecule on the MgO bilayer ($\theta = 90°$). θ is the rotation angle away from the z axis towards the x axis. Here we used $U = 6$ eV and $J = 1$ eV.

TABLE III. MAE convergence test results for different k-point meshes for representative structures on MgO substrate. The MAE values are given in meV per adatom. A negative sign of the MAE favors an out-of-plane magnetization.

k-point mesh	4×4×1	5×5×1	6×6×1	7×7×1
MAE for Co/2MgO, Fig. 1-1	−93.322	−93.547	−93.824	−93.618
MAE for CoO/2MgO, Fig. 1-2	−53.481	−53.025	−53.013	−53.157

arbitrary rotations of the magnetic moment, which is an essential ingredient for the evaluation of the MAE. Second, Liechtenstein's approach works with SOC while enabling the rotation of the magnetic moments but without having access to the structural relaxations. Thus, in practice, we perform the relaxations with the formulation of Dudarev. Once the atomic geometries are obtained, we switch to the approach of Liechtenstein *et al.* to compute the MAE. We use $U = 6\,\text{eV}$ and $J = 1\,\text{eV}$ following prior work by Ou *et al.* [44] for Co on MgO, with Rau *et al.* [11] reporting a similar U of 6.9 eV for Co on MgO via the linear response method.

In our paper, we discuss two types of simulations: 3*d* adatoms on the oxygen-top position of the MgO bilayer and 3*d* − O molecules that are either freestanding or deposited on the MgO bilayer.

For the case of freestanding 3*d*−O molecules, we employ cubic periodic cells with a lattice constant of 20 Å to minimize interactions between periodic replicas of the dimers and assume Γ-point sampling of the Brillouin zone while using different bond lengths between 3*d* adatoms and O atoms ($d_{3d\text{–}O}$).

To accommodate the 3*d* adatoms and 3*d*−O molecules on the bilayer of MgO, we used the theoretical lattice constants of a bilayer of MgO obtained from LDA (4.065 Å). We then set up 3×3 supercells such that the 3*d* adatoms are deposited on top of the oxygen positions, as shown in Fig. 1. For 3*d*−O molecules on the MgO bilayer, we placed the 3*d*−O molecules on different structures, as shown in Fig. 1. The supercells contain 73 and 74 atoms in total for the case of 3*d* adatoms on the oxygen-top position and 3*d*−O molecules deposited on the MgO bilayer, respectively, with a vacuum thickness equivalent to 9 layers of MgO.

For the MAE calculations, convergence testing was performed to ensure minimal interaction between periodic images and appropriate k-point sampling. This included testing for supercell size and k-point mesh density. The convergence tests were conducted for two representative structures: Co on MgO (structure 1) and perpendicular CoO on MgO (structure 2), as shown in Fig. 1. The results for k-point convergence testing are shown in Table III.

TABLE IV. MAE convergence test results for different supercell sizes for representative structures on MgO substrate. The MAE values are given in meV per adatom. A negative sign of the MAE favors an out-of-plane magnetization.

Supercell size	3×3	4×4
MAE for Co/2MgO, Fig. 1-1	−93.322	−90.37
MAE for CoO/2MgO, Fig. 1-2	−53.481	−56.645

Additionally, we perform supercell size convergence testing to confirm that a 3×3 supercell is sufficient to minimize interactions between periodic images. The results of the supercell size tests are presented in Table IV.

The rotation of the magnetic moment of the freestanding Co–O molecules was studied by the constrained DFT approach explained in Ref. [60]. To ensure that the different magnetic states were comparable, for each fixed magnetic configuration we perform a sequence of self-consistent constrained calculations. We highlight that the MAE obtained for the freestanding molecules are quantitatively similar when utilizing USPP or projector augmented wave (PAW) in either LSDA or the GGA, as shown in Table V.

The data needed to evaluate the conclusions in the paper are present in the text. All codes used for this work are open-source. Quantum ESPRESSO can be found at Ref. [61].

ACKNOWLEDGMENTS

Thanks Harald Brune for fruitful initial discussions on the topic of perpendicular molecules on surfaces. This work was supported by the Federal Ministry of Education and Research of Germany in the framework of the Palestinian-German Science Bridge (BMBF Grant No. 01DH16027). We acknowledge the computing time granted by the JARA-HPC Vergabegremium and VSR commission on the supercomputer JURECA at Forschungszentrum Jülich [62] and RWTH Aachen University under Project No. p0020362.

S.L. initiated, designed and supervised the project. S.S. performed the simulations and postprocessed the data. S.SA., M.d.S.D., M.A., and S.L. discussed the results. S.S. and S.L. wrote the paper to which all coauthors contributed.

The authors declare no competing interests.

TABLE V. MAE of the isolated Co–O molecule from DFT+SOC total energy calculations for different types of pseudopotentials (PPs) and exchange-correlation functionals, ($d_{Co\text{-}O} = 2$Å). The MAE values are given in meV per adatom. A negative sign of the MAE favors an out-of-plane magnetization.

PPs	GGA PAW	GGA USPP	PAW	LSDA USPP
MAE (meV)	−13.5	−12.9	−10.0	−12.84

[1] A. A. Khajetoorians, J. Wiebe, B. Chilian, and R. Wiesendanger, Realizing all-spin–based logic operations atom by atom, Science **332**, 1062 (2011).

[2] A. A. Khajetoorians, B. Baxevanis, C. Hübner, T. Schlenk, S. Krause, T. O. Wehling, S. Lounis, A. Lichtenstein, D. Pfannkuche, J. Wiebe, and R. Wiesendanger, Current-driven

spin dynamics of artificially constructed quantum magnets, Science **339**, 55 (2013).

[3] S. Loth, S. Baumann, C. P. Lutz, D. M. Eigler, and A. J. Heinrich, Bistability in atomic-scale antiferromagnets, Science **335**, 196 (2012).

[4] P. Gambardella, S. Rusponi, M. Veronese, S. Dhesi, C. Grazioli, A. Dallmeyer, I. Cabria, R. Zeller, P. Dederichs, K. Kern *et al.*, Giant magnetic anisotropy of single cobalt atoms and nanoparticles, Science **300**, 1130 (2003).

[5] C. F. Hirjibehedin, C.-Y. Lin, A. F. Otte, M. Ternes, C. P. Lutz, B. A. Jones, and A. J. Heinrich, Large magnetic anisotropy of a single atomic spin embedded in a surface molecular network, Science **317**, 1199 (2007).

[6] P. Błoński, A. Lehnert, S. Dennler, S. Rusponi, M. Etzkorn, G. Moulas, P. Bencok, P. Gambardella, H. Brune, and J. Hafner, Magnetocrystalline anisotropy energy of Co and Fe adatoms on the (111) surfaces of Pd and Rh, Phys. Rev. B **81**, 104426 (2010).

[7] F. Donati, Q. Dubout, G. Autès, F. Patthey, F. Calleja, P. Gambardella, O. V. Yazyev, and H. Brune, Magnetic moment and anisotropy of individual Co atoms on graphene, Phys. Rev. Lett. **111**, 236801 (2013).

[8] J. Hu and R. Wu, Giant magnetic anisotropy of transition-metal dimers on defected graphene, Nano Lett. **14**, 1853 (2014).

[9] I. Beljakov, V. Meded, F. Symalla, K. Fink, S. Shallcross, M. Ruben, and W. Wenzel, Spin-crossover and massive anisotropy switching of 5*d* transition metal atoms on graphene nanoflakes, Nano Lett. **14**, 3364 (2014).

[10] R. Xiao, D. Fritsch, M. D. Kuz'min, K. Koepernik, H. Eschrig, M. Richter, K. Vietze, and G. Seifert, Co dimers on hexagonal carbon rings proposed as subnanometer magnetic storage bits, Phys. Rev. Lett. **103**, 187201 (2009).

[11] I. G. Rau, S. Baumann, S. Rusponi, F. Donati, S. Stepanow, L. Gragnaniello, J. Dreiser, C. Piamonteze, F. Nolting, S. Gangopadhyay, O. R. Albertini, R. M. Macfarlane, C. P. Lutz, B. A. Jones, P. Gambardella, A. J. Heinrich, and H. Brune, Reaching the magnetic anisotropy limit of a 3*d* metal atom, Science **344**, 988 (2014).

[12] A. A. Khajetoorians and J. Wiebe, Hitting the limit of magnetic anisotropy, Science **344**, 976 (2014).

[13] S. Baumann, F. Donati, S. Stepanow, S. Rusponi, W. Paul, S. Gangopadhyay, I. G. Rau, G. E. Pacchioni, L. Gragnaniello, M. Pivetta, J. Dreiser, C. Piamonteze, C. P. Lutz, R. M. Macfarlane, B. A. Jones, P. Gambardella, A. J. Heinrich, and H. Brune, Origin of perpendicular magnetic anisotropy and large orbital moment in Fe atoms on MgO, Phys. Rev. Lett. **115**, 237202 (2015).

[14] M. Bouhassoune, M. dos Santos Dias, B. Zimmermann, P. H. Dederichs, and S. Lounis, RKKY-like contributions to the magnetic anisotropy energy: 3*d* adatoms on Pt(111) surface, Phys. Rev. B **94**, 125402 (2016).

[15] J. Ibañez-Azpiroz, M. dos Santos Dias, S. Blügel, and S. Lounis, Zero-point spin-fluctuations of single adatoms, Nano Lett. **16**, 4305 (2016).

[16] J. Ibañez-Azpiroz, M. dos Santos Dias, S. Blügel, and S. Lounis, Spin-fluctuation and spin-relaxation effects of single adatoms from first principles, J. Phys.: Condens. Matter **30**, 343002 (2018).

[17] J. Bouaziz, J. Ibañez-Azpiroz, F. S. Guimares, and S. Lounis, Zero-point magnetic exchange interactions, Phys. Rev. Res. **2**, 043357 (2020).

[18] D. Weller and A. Moser, Thermal effect limits in ultrahigh-density magnetic recording, IEEE Trans. Magn. **35**, 4423 (1999).

[19] F. Donati, S. Rusponi, S. Stepanow, C. Wckerlin, A. Singha, L. Persichetti, R. Baltic, K. Diller, F. Patthey, E. Fernandes, J. Dreiser, K. Kummer, C. Nistor, P. Gambardella, and H. Brune, Magnetic remanence in single atoms, Science **352**, 318 (2016).

[20] F. Donati, M. Pivetta, C. Wolf, A. Singha, C. Wackerlin, R. Baltic, E. Fernandes, J.-G. De Groot, S. L. Ahmed, L. Persichetti, C. Nistor, J. Dreiser, A. Barla, P. Gambardella, H. Brune, and S. Rusponi, Correlation between electronic configuration and magnetic stability in dysprosium single atom magnets, Nano Lett. **21**, 8266 (2021).

[21] S. Baumann, W. Paul, T. Choi, C. P. Lutz, A. Ardavan, and A. J. Heinrich, Electron paramagnetic resonance of individual atoms on a surface, Science **350**, 417 (2015).

[22] W. Paul, K. Yang, S. Baumann, N. Romming, T. Choi, C. Lutz, and A. Heinrich, Control of the millisecond spin lifetime of an electrically probed atom, Nat. Phys. **13**, 403 (2017).

[23] K. Yang, Y. Bae, W. Paul, F. D. Natterer, P. Willke, J. L. Lado, A. Ferrón, T. Choi, J. Fernández-Rossier, A. J. Heinrich, and C. P. Lutz, Engineering the eigenstates of coupled spin-1/2 atoms on a surface, Phys. Rev. Lett. **119**, 227206 (2017).

[24] F. D. Natterer, K. Yang, W. Paul, P. Willke, T. Choi, T. Greber, A. J. Heinrich, and C. P. Lutz, Reading and writing single-atom magnets, Nature (London) **543**, 226 (2017).

[25] P. R. Forrester, F. Patthey, E. Fernandes, D. P. Sblendorio, H. Brune, and F. D. Natterer, Quantum state manipulation of single atom magnets using the hyperfine interaction, Phys. Rev. B **100**, 180405(R) (2019).

[26] T. Choi, W. Paul, S. Rolf-Pissarczyk, A. J. Macdonald, F. D. Natterer, K. Yang, P. Willke, C. P. Lutz, and A. J. Heinrich, Atomic-scale sensing of the magnetic dipolar field from single atoms, Nat. Nanotechnol. **12**, 420 (2017).

[27] K. Yang, S.-H. Phark, Y. Bae, T. Esat, P. Willke, A. Ardavan, A. J. Heinrich, and C. P. Lutz, Probing resonating valence bond states in artificial quantum magnets, Nat. Commun. **12**, 993 (2021).

[28] P. Willke, K. Yang, Y. Bae, A. J. Heinrich, and C. P. Lutz, Magnetic resonance imaging of single atoms on a surface, Nat. Phys. **15**, 1005 (2019).

[29] P. Willke, Y. Bae, K. Yang, J. L. Lado, A. Ferrón, T. Choi, A. Ardavan, J. Fernández-Rossier, A. J. Heinrich, and C. P. Lutz, Hyperfine interaction of individual atoms on a surface, Science **362**, 336 (2018).

[30] K. Yang, P. Willke, Y. Bae, A. Ferrón, J. L. Lado, A. Ardavan, J. Fernández-Rossier, A. J. Heinrich, and C. P. Lutz, Electrically controlled nuclear polarization of individual atoms, Nat. Nanotechnol. **13**, 1120 (2018).

[31] S. Shehada, M. dos Santos Dias, F. S. M. Guimarães, M. Abusaa, and S. Lounis, Trends in the hyperfine interactions of magnetic adatoms on thin insulating layers, npj Comput. Mater. **7**, 87 (2021).

[32] S. Shehada, M. dos Santos Dias, M. Abusaa, and S. Lounis, Interplay of magnetic states and hyperfine fields of iron dimers on MgO (001), J. Phys.: Condens. Matter **34**, 385802 (2022).

[33] J. Kim, K. Noh, Y. Chen, F. Donati, A. J. Heinrich, C. Wolf, and Y. Bae, Anisotropic hyperfine interaction of surface-adsorbed single atoms, Nano Lett. **22**, 9766 (2022).

[34] L. Farinacci, L. M. Veldman, P. Willke, and S. Otte, Experimental determination of a single atom ground state orbital through hyperfine anisotropy, Nano Lett. **22**, 8470 (2022).

[35] X. Zhang, C. Wolf, Y. Wang, H. Aubin, T. Bilgeri, P. Willke, A. J. Heinrich, and T. Choi, Electron spin resonance of single iron phthalocyanine molecules and role of their non-localized spins in magnetic interactions, Nat. Chem. **14**, 59 (2022).

[36] P. Willke, T. Bilgeri, X. Zhang, Y. Wang, C. Wolf, H. Aubin, A. Heinrich, and T. Choi, Coherent spin control of single molecules on a surface, ACS Nano **15**, 17959 (2021).

[37] J. Kim, W.-j. Jang, T. H. Bui, D.-J. Choi, C. Wolf, F. Delgado, Y. Chen, D. Krylov, S. Lee, S. Yoon, C. P. Lutz, A. J. Heinrich, and Y. Bae, Spin resonance amplitude and frequency of a single atom on a surface in a vector magnetic field, Phys. Rev. B **104**, 174408 (2021).

[38] M. Steinbrecher, W. M. J. van Weerdenburg, E. F. Walraven, N. P. E. van Mullekom, J. W. Gerritsen, F. D. Natterer, D. I. Badrtdinov, A. N. Rudenko, V. V. Mazurenko, M. I. Katsnelson, A. van der Avoird, G. C. Groenenboom, and A. A. Khajetoorians, Quantifying the interplay between fine structure and geometry of an individual molecule on a surface, Phys. Rev. B **103**, 155405 (2021).

[39] A. Singha, D. Sostina, C. Wolf, S. L. Ahmed, D. Krylov, L. Colazzo, P. Gargiani, S. Agrestini, W.-S. Noh, J.-H. Park, M. Pivetta, S. Rusponi, H. Brune, A. J. Heinrich, A. Barla, and F. Donati, Mapping orbital-resolved magnetism in single lanthanide atoms, ACS Nano **15**, 16162 (2021).

[40] A. Singha, P. Willke, T. Bilgeri, X. Zhang, H. Brune, F. Donati, A. J. Heinrich, and T. Choi, Engineering atomic-scale magnetic fields by dysprosium single atom magnets, Nat. Commun. **12**, 4179 (2021).

[41] K. Yang, W. Paul, S.-H. Phark, P. Willke, Y. Bae, T. Choi, T. Esat, A. Ardavan, A. J. Heinrich, and C. P. Lutz, Coherent spin manipulation of individual atoms on a surface, Science **366**, 509 (2019).

[42] S. Kovarik, R. Robles, R. Schlitz, T. S. Seifert, N. Lorente, P. Gambardella, and S. Stepanow, Electron paramagnetic resonance of alkali metal atoms and dimers on ultrathin MgO, Nano Lett. **22**, 4176 (2022).

[43] H. Garai-Marin, M. dos Santos Dias, S. Lounis, J. Ibañez-Azpiroz, and A. Eiguren, Microscopic theory of spin relaxation of a single Fe adatom coupled to substrate vibrations, Phys. Rev. B **107**, 144417 (2023).

[44] X. Ou, H. Wang, F. Fan, Z. Li, and H. Wu, Giant magnetic anisotropy of Co, Ru, and Os adatoms on MgO (001) surface, Phys. Rev. Lett. **115**, 257201 (2015).

[45] D.-s. Wang, R. Wu, and A. Freeman, First-principles theory of surface magnetocrystalline anisotropy and the diatomic-pair model, Phys. Rev. B **47**, 14932 (1993).

[46] H. Brooks, Ferromagnetic anisotropy and the itinerant electron model, Phys. Rev. **58**, 909 (1940).

[47] P. Bruno, Tight-binding approach to the orbital magnetic moment and magnetocrystalline anisotropy of transition-metal monolayers, Phys. Rev. B **39**, 865 (1989).

[48] D. Dai, H. Xiang, and M.-H. Whangbo, Effects of spin-orbit coupling on magnetic properties of discrete and extended magnetic systems, J. Comput. Chem. **29**, 2187 (2008).

[49] J. J. Sakurai, E. D. Commins, and S. F. Tuan, Modern quantum mechanics, revised edition, Am. J. Phys. **63**, 93 (1995).

[50] Y. Lu, X. Zuo, M. Feng, and T. Zhou, Magnetic anisotropy in the boron nitride monolayer doped by 3d transitional metal substitutes at boron-site, J. Appl. Phys. **113**, 17C304 (2013).

[51] B. Shao, M. Feng, and X. Zuo, Carrier-dependent magnetic anisotropy of cobalt doped titanium dioxide, Sci. Rep. **4**, 7496 (2014).

[52] G. van der Laan, $M_{2,3}$ absorption spectroscopy of 3d transition-metal compounds, J. Phys.: Condens. Matter **3**, 7443 (1991).

[53] D. Vanderbilt, Soft self-consistent pseudopotentials in a generalized eigenvalue formalism, Phys. Rev. B **41**, 7892 (1990).

[54] A. D. Corso and A. M. Conte, Spin-orbit coupling with ultrasoft pseudopotentials: Application to Au and Pt, Phys. Rev. B **71**, 115106 (2005).

[55] A. D. Corso, Pseudopotentials periodic table: From H to Pu, Comput. Mater. Sci. **95**, 337 (2014).

[56] J. P. Perdew and A. Zunger, Self-interaction correction to density-functional approximations for many-electron systems, Phys. Rev. B **23**, 5048 (1981).

[57] A. Liechtenstein, V. I. Anisimov, and J. Zaanen, Density-functional theory and strong interactions: Orbital ordering in Mott-Hubbard insulators, Phys. Rev. B **52**, R5467 (1995).

[58] S. L. Dudarev, G. A. Botton, S. Y. Savrasov, C. J. Humphreys, and A. P. Sutton, Electron-energy-loss spectra and the structural stability of nickel oxide: An LSDA+U study, Phys. Rev. B **57**, 1505 (1998).

[59] M. Cococcioni and S. de Gironcoli, Linear response approach to the calculation of the effective interaction parameters in the LDA+U method, Phys. Rev. B **71**, 035105 (2005).

[60] P.-W. Ma, S. L. Dudarev, Constrained density functional for noncollinear magnetism, Phys. Rev. B **91**, 054420 (2015).

[61] https://www.quantum-espresso.org/download.

[62] Jülich Supercomputing Centre, J. Large-Scale Res. Facilities **4**, A132 (2018).